HHS Public Access

Author manuscript

Mol Cancer Res. Author manuscript; available in PMC 2018 May 14.

Published in final edited form as:

Mol Cancer Res. 2018 January ; 16(1): 69–77. doi:10.1158/1541-7786.MCR-17-0260.

Functional Impact of Chromatin Remodeling Gene Mutations and Predictive Signature for Therapeutic Response in Bladder Cancer

Jason E. Duex[1], **Kalin E Swain**[1], **Garrett M. Dancik**[2], **Richard D. Paucek**[1], **Charles Owens**[1], **Mair E.A. Churchill**[3], and **Dan Theodorescu**[1,3,4]

[1]Department of Surgery (Urology), University of Colorado, Aurora, Colorado

[2]Department of Computer Science, Eastern Connecticut State University, Willimantic, Connecticut

[3]Department of Pharmacology, University of Colorado, Aurora, Colorado

[4]University of Colorado Comprehensive Cancer Center, Aurora, Colorado

Abstract

Urothelial carcinoma accounts for most of the bladder cancer cases. Using next-generation sequencing (NGS) technology, we found that a significant percentage (83%) of tumors had mutations in chromatin-remodeling genes. Here, we examined the functional relevance of mutations in two chromatin-remodeling genes, EP300 and its paralog, CREBBP, which are mutated in almost one-third of patients. Interestingly, almost half of missense mutations cluster in the histone-acetyltransferase (HAT) domain of EP300/CREBBP. This domain catalyzes the transfer of an acetyl group to target molecules such as histones, thereby regulating chromatin dynamics. Thus, patients with EP300 or CREBBP mutations may have alterations in the ability of the corresponding proteins to modify histone proteins and control transcriptional profiles. In fact, it was determined that many of the missense HAT mutations in EP300 (64%) and CREBBP (78%) were HAT-inactivating. These inactivating mutations also correlated with invasive disease in patients. Strikingly, the prediction software Mutation Assessor accurately predicted the functional consequences of each HAT missense mutation. Finally, a gene expression signature was developed that associated with loss of HAT activity and that this signature was associated with more aggressive cancer in four patient datasets. Further supporting the notion that this score accurately

Corresponding Author: Dan Theodorescu, University of Colorado Comprehensive Cancer Center, 13001 E. 17th Place, F-434, Building 500, Room C6004, Aurora, CO 80045. Phone: 303-724-7135; Fax: 303-724-3162; dan.theodorescu@ucdenver.edu.
J.E. Duex and K.E. Swain contributed equally to this article.

Disclosure of Potential Conflicts of Interest No potential conflicts of interest were disclosed.

Authors' Contributions Conception and design: J.E. Duex, K.E. Swain, D. Theodorescu
Development of methodology: J.E. Duex, K.E. Swain

Note: Supplementary data for this article are available at Molecular Cancer Research Online (http://mcr.aacrjournals.org/).

Acquisition of data (provided animals, acquired and managed patients, provided facilities, etc.): J.E. Duex, K.E. Swain, C. Owens, R.D. Paucek
Analysis and interpretation of data (e.g., statistical analysis, biostatistics, computational analysis): J.E. Duex, K.E. Swain, G.M. Dancik, M.E.A. Churchill, D. Theodorescu
Writing, review, and/or revision of the manuscript: J.E. Duex, K.E. Swain, G.M. Dancik, M.E.A. Churchill, D. Theodorescu
Administrative, technical, or material support (i.e., reporting or organizing data, constructing databases): D. Theodorescu
Study supervision: J.E. Duex, D. Theodorescu

reflects HAT activity, we found it is responsive to treatment of cancer cells to mocetinostat, a histone deacetylase (HDAC) inhibitor.

Implication—This study provides a rationale for targeted sequencing of EP300 and CREBBP and use of a gene profiling signature for predicting therapeutic response in patients.

Introduction

In 2016, approximately 16,000 Americans succumbed to bladder cancer (1), a disease which is associated with a cost per patient from diagnosis to death of approximately $150K, among the highest of any cancer (2). For most of these patients, the cause of death is attributable to metastatic spread of the cancer. We and others have used next-generation sequencing (NGS) technology to identify the mutational spectrum of urothelial carcinomas of the bladder with the hope that this will provide therapeutic insights and actionable targets. To date, four independent studies performed whole-genome and whole-exome sequencing in bladder tumor samples to catalog genetic alterations to identify the dysregulated signaling pathways of bladder cancer tumorigenesis and metastasis (3–6). These studies revealed high alteration frequencies in genes participating in chromatin remodeling. In particular, 83% of patients in one study exhibited mutations in the chromatin remodeling genes (6) while our previous study identified *EP300* and *CREBBP* as 2 of the 4 most frequently mutated genes in human bladder cancer (7).

The gene products of *EP300* (p300) and *CREBBP* (CBP) were originally discovered to bind to the adenoviral E1A protein and the cAMP-response-element-binding (CREB) protein, respectively (8, 9). *EP300* and *CREBBP* are well studied transcriptional coactivators (5), with histone acetyltransferase (HAT) and ubiquitin ligase activity (8, 10). Owing to their multi-domain architecture, these highly conserved mammalian transcriptional coactivators have been implicated in many cellular processes such as cell proliferation, differentiation, development, DNA damage repair, and apoptosis (11). The ability of p300 and CBP to remodel chromatin is due to their HAT activity. We found that, in bladder cancer in particular, the HAT domain in tumors is mutated at a much higher rate than the rest of the gene, suggesting that activity of this domain has a major impact on tumorigenicity. Thus, we set out to determine the functional impact of the HAT domain mutations on p300 and CBP acetyltransferase activity. Surprisingly, we found that not all mutations lead to changes in HAT activity. However, we were able to show that the activity of a particular type of mutation was predicted with 100% accuracy in our dataset using Mutation Assessor software. Furthermore, we identified a gene signature associated with HAT inactivity in p300 and CBP and from this, determined that loss of HAT activity is associated with the more aggressive bladder cancer in patients.

Materials and Methods

Cell culture

The human bladder cancer cell lines VMCUB1 and UMUC3 clone 31 (a clone of UMUC3 with diminished p300 and CBP protein levels), as well as the HEK293T cell line were obtained from the University of Colorado Cancer Center (UCCC, Aurora, CO) and

immediately frozen to multiple ampules. These cell lines from UCCC had been fingerprinted by short tandem repeat (STR) profiling (Qiagen) and shown to be free of mycoplasma contamination (Lonza). Thawed cells were used in experiments within 4 weeks of being thawed to minimize genetic drift and contamination. Bladder cancer lines were maintained in MEM (Invitrogen) supplemented with 10% FBS and 1% penicillin–streptomycin (Life Technologies) while HEK 293T cells were maintained in DMEM (Invitrogen) supplemented with 10% FBS. All cell lines grew in a 37°C and 5% CO_2 incubator. All transfection reactions were carried out in their growth media.

Antibodies

Antibodies include the Acetyl-Histone H3 Antibody Sampler Kit and H3-K23Ac (Cell Signaling Technology), P300 (C-20, Santa Cruz Biotechnology), CBP (A-22, Santa Cruz Biotechnology), α-tubulin (EMD Millipore), AR (D6F11, Cell Signaling Technology), acetyl-lysine (9441, Cell Signaling Technology), and horseradish peroxidase-linked (HRP) secondary antibody (Cell Signaling Technology). Enhanced chemiluminescent (ECL) substrates include SuperSignal West Pico and Femto (Pierce).

Plasmid cloning

pcDNA3.1-p300 (Addgene #23252) encoding *H. sapiens EP300* was digested with *Bgl*II to yield three fragments, vector backbone and two fragments containing P300 coding sequence (4 and 8 kb). The 8-kb fragment was CIP-treated (NEB) then ligated into pUC19 for site-directed mutagenesis with mutagenic primers. Site-directed mutagenesis was carried out using the Quikchange II XL Site-directed Mutagenesis Kit (Agilent Technologies). After confirmation by DNA sequencing, it was redigested with *Bgl*II, and together with the 4 kb-EP300 fragment, ligated back into the original vector and fragment orientation confirmed with a *Nde*I restriction digest. pcDNA3β-FLAG-CBP-HA (Addgene #32908) encoding *M. musculus Crebbp* was sequentially digested with *Sma*I then *Kpn*I to isolate a 3,194-bp CBP fragment that was ligated into pUC19 for site-directed mutagenesis. The resultant pUC19 plasmid with correct CBP mutagenic sites was redigested with *Sma*I–*Kpn*I and then ligated back into the original vector. The full-length mutated CBP ORF was then transferred into a pIR-ESPuro3 vector by PCR amplification (CloneAmp HiFi PCR premix; Clontech) of the gene in two halves before different reactions before ligating into a *Bam*HI and *Not*I cut pIRESPuro3 using InFusion HD Cloning Kit (Clontech). For both P300 and CBP cloning strategies, the final transformants in bacteria were isolated using the EndoFree Plasmid Maxiprep Kit (Qiagen) to purify plasmid DNA followed by DNA sequencing.

DNA transfections

Cells grown in 6-well plates were transfected with 1 μg plasmid DNA using either Lipofectamine 2000 (Invitrogen) or X-tremeGENE 9 (Roche) according to the manufacturer's instructions. The lipid–DNA complexes were replaced with media 4–6 hours posttransfection. To prevent histone deacetylation, Trichostatin A (TSA, Sigma) was added to the cells overnight. Cells were maintained in medium for a total of 48 hours prior to making whole-cell lysates.

Whole-cell lysates, SDS-PAGE, and immunoblotting

Cells were washed with ice-cold PBS, then lysed in ice-cold RIPA lysis buffer [50 mmol/L Tris-HCL, pH 8, 150mmol/L NaCl, 0.1% NaCl, 0.1% SDS, 1% IGEPAL CA-630 and protease inhibitors (Sigma)] for 20 minutes at 4°C. Lysates were cleared by centrifugation (16,000 × *g*, 20 minutes, 4°C). Total protein concentration was determined using the BCA Protein Assay Kit (Pierce). Whole-cell protein extracts were denatured in SDS sample buffer (Boston Bioproducts) containing 2.5% BME and heated to 95°C for 5 minutes. Samples were subjected to SDS-PAGE using a 5%–20 % gradient acrylamide gel (Bio-Rad) and then transferred onto PVDF membrane using a Trans-blot Turbo transfer system (Bio-Rad). Image acquisition was carried out using the Bio-Rad Chemidoc MP imaging systems. Using Image Lab software, each band was quantified and then normalized to a respective internal control (Histone-3 or α-Tubulin).

Computation-based structural modeling and bioinformatics

The program Phyre2was used to build a 3D model for CBP HAT domain based on 3BIY[23]. Structural analyses of missense mutants was performed by visual inspection using PyMol. The Catalogue Of Somatic Mutations In Cancer (COSMIC) dataset was accessed at cancer.sanger.ac.uk. Mutation and expression data from The Cancer Genome Atlas (TCGA) bladder cancer cohort were downloaded from cBioPortal using the CGDS-R (12) package and analyzed in R (www.r-project.org). Patients were categorized as HAT mutant if they had missense mutations or deletions in the HAT domain (positions 1306–1627 for *CREBBP*; positions 1342–1649 for EP300), or frameshift or nonsense mutations upstream of the HAT domain. Patients were classified as wild-type if they had no CREBBP or EP300 mutations. In the TCGA cohort, genes were removed if more than 20% of values were missing or more than 30% of read counts were zero. The nonparametric Wilcoxon rank-sum test was used to identify differentially expressed genes at $P < 0.001$. Gene expression data for MDA-MB-231 cell lines treated with mocetinostat, and for the CNUH, DFCI, and Lindgren cohorts were downloaded from the Gene Expression Omnibus (13), and are available from accession numbers GSE65495, GSE13507, GSE31684, and GSE32548, respectively. Gene expression data for MSKCC was downloaded from supplementary material to publication (14). For each gene, expression values were normalized across samples in each cohort to have mean zero and SD one. For genes with multiple probes, the probe with the highest mean expression was used (15). The HAT inactivation score is the sum of (normalized) expression values for upregulated genes in HAT-mutant samples minus the sum of (normalized) expression values of all downregulated genes in HAT-mutant samples. The two-sample *t* test was used to evaluate the ability of HAT inactivation scores to distinguish between wild-type and mutant samples, and between patients with nonmuscle-invasive and muscle-invasive tumors, and between cells treated with mocetinostat and controls. Individual genes were evaluated for the ability to distinguish between muscle-invasive and nonmuscle-invasive tumors using the Bladder Cancer Biomarker Evaluation Tool (16). Fisher combined probability test is used to combine *P* values obtained from individual cohorts. Protein–protein interaction networks were identified using STRING, version 10.5 (17).

Results

EP300 and CREBBP are mutated in bladder cancer more than other cancers

Here, we show *EP300* (Fig 1A) and *CREBBP* (Fig 1B) are mutated in human bladder cancer more so than any other cancer type. These data suggest that assessing human patient mutations of *EP300* and *CREBBP* in bladder cancer models will likely have more clinical significance. Analysis of amino acid substitutions in *EP300* from the COSMIC dataset (18) reveals that the HAT domain is by far the most mutated domain in all cancer types (Fig. 1C). Hence, we investigated the distribution of *EP300* mutations using cBioPortal for Cancer Genomics (19, 20) as this would also allow us to correlate specific mutations with patient data. Using bladder cancer specifically in cBioPortal revealed that there is a concentration of mutations within the HAT domain (Fig. 1C). It is worth noting that nearly all nonsense mutations are upstream of HAT domain and the protein products, even if stable, would be lacking HAT activity. Analysis of *CREBBP* mutations using COSMIC and cBioPortal revealed similar observations to those of *EP300* (Fig. 1D). Thus, bladder cancer appears to be the most relevant model to determining the functional impact of *EP300* and *CREBBP* patient mutations on HAT activity.

HAT domain missense mutations have differing effects on HAT domain activity

The human bladder cancer patient data available through TCGA identifies 11 different *EP300* missense mutations (at 10 different amino acid positions) and 9 *CREBBP* missense mutations (at 7 different amino acid positions) in the HAT domain, with only one instance of a shared mutation between the two proteins (Fig. 2A). This shared mutation, however, is the most common missense mutation in both genes and lead to changes at the D1399 (p300 protein) and D1435 (CBP protein) positions (Fig. 2A). Our study set out to characterize the functional impact these HAT domain mutations have on the ability of p300 and CBP to transfer an acetyl residue to its primary substrate, HistoneH3. We first mutated a plasmid encoding the cDNA for the *EP300* gene, introducing one of the 11 missense mutations, and then expressing the plasmid in two human bladder cancer cell lines, as well as HEK293 cells, to assess HAT activity. After screening 40 bladder cancer cell lines for endogenous p300 and CBP protein levels, we chose VMCUB1 and a clone of UMUC3 due to their low levels of endogenous p300 and CBP protein expression. The HEK293T cell line was also used because of its low endogenous p300 and CBP protein levels. Forty-eight hours after transfection, total cell lysates of the cells were analyzed by Western blot analysis to determine the extent to which HistoneH3 was acetylated at lysine 27 (K27). HistoneH3 acetylation at K9, K14, K18, K23, K27, and K56 was assessed and K27 was chosen as it provided the best dynamic range (Supplementary Fig. S1). Using this assay, we were able to see that overexpression of wild-type p300 protein in 3 different human cell lines leads to a 5- to 8-fold increase in HistoneH3-K27 acetylation relative to control cells expressing vector alone (Fig. 2B). In addition, we assessed the impact of a known p300 HAT-inactive mutant, D1399Y (21), and as expected observed only baseline levels of acetylation of K27 on HistoneH3 (Fig. 2B).Thus, this assay was robust enough to assess HAT domain activity with single amino acid changes in the HAT domain.

In assessing the patient-directed missense mutations in the bladder cancer line VMCUB1, we found that HAT domain activity was lost in 7 of the 11 patient-identified mutations (Fig. 2B). Interestingly, 4 of the patient-identified mutations behaved like wild-type. These same observations were also observed in the other 2 human cell lines tested. So, despite a patient having a missense mutation specifically in the HAT domain, it does not necessarily lead to an inactivation of the acetyltransferase function of p300. Thus, this data suggests that it would be prudent to biologically determine the functional impact of a mutation found in the HAT domain of *EP300*.

We also determined acetyltransferase activities for 9 patient *CREBBP* HAT domain mutations. As observed with wild-type p300 overexpression, wild-type CBP overexpression lead to a dramatic (5–9 fold) increase in HistoneH3-K27 acetylation (Fig. 2C).Consistent with the literature (22), overexpression of a known CBP HAT–inactive mutant, D1435E, lead to no increase in HistoneH3-K27 acetylation (Fig. 2C). Assessing the patient-directed mutations in VMCUB1 cells revealed that, like the p300 analysis above, most but not all mutations lead to inactivation of the acetyltransferase activity on HistoneH3 (Fig. 2C). Similar observations were made using two other human cell lines.

Computational prediction of the functional impact of EP300 and CREBBP mutation

The observation that not all p300 or CBP patient HAT domain missense mutations lead to inactivation of acetyltransferase activity suggests that biologic determination of a mutation would need to be performed before assigning functionality to the protein products. However, this would be very burdensome in the realm of patient diagnoses and prognoses and thus we sought an alternative method for determining the functional impact of HAT domain missense mutations. With this in mind, we investigated the accuracy of a well-known functional predictor of missense mutations, Mutation Assessor software (23). In averaging the HistoneH3-K27 acetylation data for p300 in all three cell lines (Fig. 3A), we found a 100% correlation between HAT domain inactivity and a "high" functional impact label from Mutation Assessor (Fig. 3A). Conversely, a "low" or "medium" functional impact label had 100% correlation with mutants which retained HistoneH3-K27 acetylation activity. A similar observation was made when assessing the CBP HistoneH3-K27 acetylation data where again, there was 100% correlation between the Mutation Assessor prediction and HAT domain activity on HistoneH3-K27 acetylation (Fig. 3B). When plotting the change in H3-Ac27 activity between a missense mutant and wild-type against the Mutation Assessor functional impact label, we again see a strong correlation between enzyme activity and Mutation Assessor functional impact calling (Fig. 3C). We assessed this mathematically by assigning a score of 3 to high, 2 to medium, and 1 to low Mutation Assessor functional impact labels and plotting (Fig. 3D). This analysis revealed a strong correlation (Pearson coefficient = 0.8918, $P < 0.0001$) between Mutation Assessor functional impact calling and the functional effect of missense mutations in the HAT domain of *EP300* and *CREBBP*.

Functional predictions of patient mutations using HAT domain crystal structure

The structures of p300 HAT domain bound to various ligands have been solved by X-ray crystallography (21, 24, 25). This afforded us the ability to molecularly interpret the patient-directed mutations and assess their correlation with the crystal structure. As all the p300

HAT domain crystal structures are similar, we chose to carry out our analysis using the first published p300 HAT crystal structure, 3BIY (24). We assessed the likely consequences of the HAT mutations by examining the p300 structure bound to a bisubstrate inhibitor. Residues D1399, H1451, and Q1455 whose variation leads to HAT inactivation, form a highly interconnected network of hydrogen bonding, van der Waals, and ionic interactions directly with the phosphopantetheine moiety of the lysyl CoA complex within the "L1" substrate binding loop (Fig. 4A, i). R1627, another residue whose variation leads to HAT inactivation, also has interactions linking its loop (carbonyl oxygen of Y1446) to the carbonyl oxygen of the lysine substrate (Fig. 4A, ii). Any substitution at these residues would be expected to alter their position in the active site and reduce substrate binding. Indeed, in previous mutational analysis, D1399 was shown to be crucial for catalytic activity (24). For the other two residues in our bladder cancer patient dataset, whose variation we show leads to HAT inactivation (C1385 and D1485), the effects are most likely to be due to decreased stability of the HAT domain (Fig. 4A, iii and iv). Substitution of C1385 with tyrosine would create steric hindrance, and substitution of the D1485 with valine would abolish stabilizing ionic interactions with the neighboring lysines and a helix dipole distal to the substrate binding cleft. Four bladder cancer patient mutations within the HAT domain did not abolish histone acetylation activity. From our analysis, a L1409 substitution with phenylalanine would not disrupt any interactions (Fig. 4A, i). Residues E1521, E1526, and K1554 lie in the "auto-acetylation" loop, which was not present in the crystal structure (Fig. 4A, iii). The same p300 loop-deletion mutant as in 3BIY is catalytically active (21, 24, 25).

To assess the likely functions of the CBP missense mutants, we produced a homology model from the highly similar p300 structure as there is no CBP structure. Our *in vitro* assay identified 5 CBP HAT-inactivating positions (D1435, S1436, R1446, F1484, and W1502), which cluster near the Lys-CoA molecule in the model (Fig. 4B, i). Residues D1435 and S1436 form a highly interconnected network of hydrogen bonding, van der Waals, and ionic interactions directly with the Lys-CoA within the "L1" substrate binding loop, whereas R1446 binds directly to the phosphate group of the ligand (Fig. 4B, ii). Both F1484 and W1502 are buried in different hydrophobic pockets and substitutions to these residues would likely destabilize the entire HAT domain (Fig. 4B, i and ii). Two of the missense mutations that had no negative impact on HAT activity, D1481G and S1687F, can be tolerated because they occur in surface-exposed residues that do not have direct interactions with the active site (Fig. 4B). In conclusion, the activities of the missense mutants are readily explained by their structural roles in the CBP model

A HAT domain activity gene signature correlates with advanced disease in bladder cancer patients

To assess the impact of HAT inactivation status in additional patient datasets where mutation status for *EP300* or *CREBBP* is unknown, a HAT inactivation signature was developed. Our analysis revealed that 16 genes were differentially expressed ($P < 0.001$) between individuals with inferred HAT-inactivating mutations (see Materials and Methods) in *CREBBP* or *EP300* ($n = 21$) and individuals with wild-type status ($n = 91$) in the TCGA cohort (Fig 5A). This gene expression signature was then used to calculate a "HAT inactivation" score, where high scores are associated with loss of HAT activity and low

scores are associated with wild-type activity ($P < 0.001$; Fig. 5B). The clinical relevance of the HAT inactivation signature was then evaluated by looking at its association with bladder cancer stage and outcome. Using data from four additional bladder cancer cohorts ($n = 479$), we found that patients with muscle-invasive tumors had higher HAT inactivation scores than patients with nonmuscle-invasive tumors ($P < 0.05$; Fig 5C). However, neither the inferred HAT inactivation status nor the HAT inactivation signature was predictive of outcome, indicating that HAT activity alone is not prognostic in bladder cancer (Supplementary Figs. S2 and S3A). Interestingly, when we focused on genes within the HAT inactivation signature whose protein products are known to experimentally interact with *EP300* or *CREBBP* gene products (Supplementary Fig. S3B), we found that the expression of the HAT inactivation signature gene *Elk1* was associated with outcome in two patient cohorts (Supplementary Fig. S3C).

In bladder cancer, there is an ongoing clinical trial evaluating the histone deacetylase (HDAC) inhibitor mocetinostat, in patients with mutations in *CREBBP/EP300* (NCT02236195). We therefore evaluated whether our HAT inactivation signature was inversely associated with mocetinostat treatment, as such a relationship would support further exploration of the HAT inactivation signature as a candidate biomarker for identifying likely responders to this treatment. In an analysis of gene expression profiles of MDA-MB-231 breast cancer cells treated with mocetinostat (26), we found that HAT inactivation scores decrease following treatment (Fig. 5D; $P = 0.053$), consistent with mocetinostat counteracting the effects of lost p300/CBP HAT activity. In that study, the group reported the top 6 upregulated and top 6 downregulated genes following mocetinostat treatment (26). To assess the utility of this treatment in bladder cancer, genes up- or downregulated following mocetinostat treatment were evaluated for association with stage in bladder cancer in 12 patient cohorts ($n = 1,362$), using the Bladder Cancer Biomarker Evaluation Tool (16). The top 6 genes found to be downregulated following treatment were found in bladder cancer patients to be significantly ($P < 0.05$) upregulated in invasive tumors (Fig. 5E; Supplementary Table S1). Such an observation supports the notion of mocetinostat as a therapeutic possibility for bladder cancer patients and may have a greater benefit in patients with muscle-invasive disease. Of the 6 upregulated genes reported in the mocetinostat study, 3 have not been profiled in any dataset, and the remaining 3 did not show a consistently significant association with stage (Supplementary Table S1). However, drawing any firm conclusions from these 3 upregulated genes is difficult given how few datasets reported expression data for the genes.

Discussion

The chromatin-remodeling genes *EP300* and *CREBBP* are commonly mutated with bladder cancer tumors exhibiting the highest percentage. Therefore, we felt this cancer type was ideal to assess whether the abundance of HAT domain mutations observed in these two genes are associated with clinical outcome in patients. Surprisingly, we discovered that not all HAT domain mutations lead to loss of HAT activity. This suggests that each mutation observed in a tumor would need to be assessed biologically before determining its prognostic impact and assigning potential therapeutic approaches for the patient.

However, as this would be quite burdensome, we sought to investigate alternatives to biological determination of function, we investigated bioinformatic methods for predicting functional impacts of mutations. We discovered that there existed a 100% qualitative correlation between our empirical data on 22 HAT domain variants and the corresponding prediction from the program Mutation Assessor. Moreover, these results correlated well with our structural analyses. While prior studies have assessed the accuracy of Mutation Assessor and other prediction programs (27) using literature-based confirmations, our study is one of the few who have directly compared individual empirical data with Mutation Assessor predictions. Owing to the ever-increasing accessibility to NGS for cancer patients and the slow rate of biological investigation of identified variants, it will be critical going forward to develop methods to predict the functional impact the variants. The work presented here contributes to that cause by validating the abilities of programs such as Mutation Assessor, illustrating the potential contributions of biophysical structural interpretations.

Another approach to determining prognosis for a patient when no biological data exists for their specific *EP300* or *CREBBP* variant is to identify a gene signature that is significantly associated with loss of p300 or CBP HAT activity. Here we were able to identify a HAT inactivation gene signature and also found that it correlated with a more aggressive, muscle-invasive disease in bladder cancer patients. One of the more intriguing members of this signature is the gene *Elk1*. We found this gene to be upregulated with loss of HAT activity and interestingly, Elk1 activity has been previously shown to be dependent on CBP (28) and p300 (29) physical association and cooperation. The HAT inactivation signature identified in our study includes an increase in Elk1 expression being associated with advanced bladder cancer disease. Consistent with our signature, Elk1 upregulation was found to be associated with tumor progression in bladder cancer (30). Such findings lend additional support to the clinical relevance of our HAT inactivation signature. Additional sequencing data from bladder cancer patients may further refine this signature and enhance its predictive ability.

The relevance of our gene signature is further supported by recent work with mocetinostat. This drug targets histone deacetylase enzymes with the goal of maintaining appropriate levels of histone acetylation, levels which may be insufficient in patients lacking normal histone acetyltransferase (HAT) activity. To be eligible in a current phase II trial (NCT02236195) bladder cancer patients must have genetic alterations of *EP300* or *CREBBP*. However, given our data, the presence of a mutation does not ensure loss of HAT activity and highlights the utility of our gene signature for stratifying patients in this trial and others premised on the same principle that loss of HAT activity will make patients more responsive to histone deacetylase inhibitors such as mocetinostat. Taken together, here we provide new biological insights and tools that could potentially be used to guide prognosis and therapy in patients with *EP300* and *CREBBP* alterations.

Supplementary Material

Refer to Web version on PubMed Central for supplementary material.

Acknowledgments

The authors thank the Protein Production/Tissue Culture/MoAB Shared Resource (PPSR) of the University of Colorado Cancer Center for providing cell lines and cell line authentication.

Grant Support

This work was supported by NIH grant CA143971 (to D. Theodorescu). The PPSR receives support from the National Cancer Institute through the Cancer Center Support grant (P30CA046934).

References

1. Siegel RL, Miller KD, Jemal A. Cancer statistics, 2016. CA Cancer J Clin. 2016; 66:7–30. [PubMed: 26742998]
2. Avritscher EBC, Cooksley CD, Grossman HB, Sabichi AL, Hamblin L, Dinney CP, et al. Clinical model of lifetime cost of treating bladder cancer and associated complications. Urology. 2006; 68:549–53. [PubMed: 16979735]
3. Cancer Genome Atlas Research Network. Comprehensive molecular characterization of urothelial bladder carcinoma. Nature. 2014; 507:315–22. [PubMed: 24476821]
4. Guo G, Sun X, Chen C, Wu S, Huang P, Li Z, et al. Whole-genome and whole-exome sequencing of bladder cancer identifies frequent alterations in genes involved in sister chromatid cohesion and segregation. Nat Genet. 2013; 45:1459–63. [PubMed: 24121792]
5. Iyer G, Al-Ahmadie H, Schultz N, Hanrahan AJ, Ostrovnaya I, Balar AV, et al. Prevalence and co-occurrence of actionable genomic alterations in high-grade bladder cancer. J Clin Oncol. 2013; 31:3133–40. [PubMed: 23897969]
6. Kim PH, Cha EK, Sfakianos JP, Iyer G, Zabor EC, Scott SN, et al. Genomic predictors of survival in patients with high-grade urothelial carcinoma of the bladder. Eur Urol. 2015; 67:198–201. [PubMed: 25092538]
7. Gui Y, Guo G, Huang Y, Hu X, Tang A, Gao S, et al. Frequent mutations of chromatin remodeling genes in transitional cell carcinoma of the bladder. Nat Genet. 2011; 43:875–8. [PubMed: 21822268]
8. Eckner R, Ewen ME, Newsome D, Gerdes M, DeCaprio JA, Lawrence JB, et al. Molecular cloning and functional analysis of the adenovirus E1A-associated 300-kD protein (p300) reveals a protein with properties of a transcriptional adaptor. Genes Dev. 1994; 8:869–84. [PubMed: 7523245]
9. Kwok RP, Lundblad JR, Chrivia JC, Richards JP, Bächinger HP, Brennan RG, et al. Nuclear protein CBP is a coactivator for the transcription factor CREB. Nature. 1994; 370:223–6. [PubMed: 7913207]
10. Chrivia JC, Kwok RP, Lamb N, Hagiwara M, Montminy MR, Goodman RH. Phosphorylated CREB binds specifically to the nuclear protein CBP. Nature. 1993; 365:855–9. [PubMed: 8413673]
11. Wang F, Marshall CB, Ikura M. Transcriptional/epigenetic regulator CBP/ p300 in tumorigenesis: structural and functional versatility in target recognition. Cell Mol Life Sci. 2013; 70:3989–4008. [PubMed: 23307074]
12. Jacobsen, A. cgdsr: R-Based API for Accessing the MSKCC Cancer Genomics Data Server (CGDS). R package version 1.2.5. [Internet]. 2015. Available from: https://CRAN.R-project.org/package=cgdsr
13. Barrett T, Troup DB, Wilhite SE, Ledoux P, Evangelista C, Kim IF, et al. NCBI GEO: archive for functional genomics data sets–10 years on. Nucleic Acids Res. 2011; 39(Database issue):D1005–1010. [PubMed: 21097893]
14. Sanchez-Carbayo M, Socci ND, Lozano J, Saint F, Cordon-Cardo C. Defining molecular profiles of poor outcome in patients with invasive bladder cancer using oligonucleotide microarrays. J Clin Oncol. 2006; 24:778–89. [PubMed: 16432078]
15. Miller JA, Cai C, Langfelder P, Geschwind DH, Kurian SM, Salomon DR, et al. Strategies for aggregating gene expression data: the collapseRows R function. BMC Bioinformatics. 2011; 12:322. [PubMed: 21816037]

16. Dancik GM. An online tool for evaluating diagnostic and prognostic gene expression biomarkers in bladder cancer. BMC Urol. 2015; 15:59. [PubMed: 26126604]
17. Szklarczyk D, Morris JH, Cook H, Kuhn M, Wyder S, Simonovic M, et al. The STRING database in 2017: quality-controlled protein-protein association networks, made broadly accessible. Nucleic Acids Res. 2017; 45:D362–8. [PubMed: 27924014]
18. Forbes SA, Beare D, Gunasekaran P, Leung K, Bindal N, Boutselakis H, et al. COSMIC: exploring the world's knowledge of somatic mutations in human cancer. Nucleic Acids Res. 2015; 43(Database issue):D805–811. [PubMed: 25355519]
19. Cerami E, Gao J, Dogrusoz U, Gross BE, Sumer SO, Aksoy BA, et al. The cBio cancer genomics portal: an open platform for exploring multidimensional cancer genomics data. Cancer Discov. 2012; 2:401–4. [PubMed: 22588877]
20. Gao J, Aksoy BA, Dogrusoz U, Dresdner G, Gross B, Sumer SO, et al. Integrative analysis of complex cancer genomics and clinical profiles using the cBioPortal. Sci Signal. 2013; 6:pl1. [PubMed: 23550210]
21. Delvecchio M, Gaucher J, Aguilar-Gurrieri C, Ortega E, Panne D. Structure of the p300 catalytic core and implications for chromatin targeting and HAT regulation. Nat Struct Mol Biol. 2013; 20:1040–6. [PubMed: 23934153]
22. Pasqualucci L, Dominguez-Sola D, Chiarenza A, Fabbri G, Grunn A, Trifonov V, et al. Inactivating mutations of acetyltransferase genes in B-cell lymphoma. Nature. 2011; 471:189–95. [PubMed: 21390126]
23. Reva B, Antipin Y, Sander C. Predicting the functional impact of protein mutations: application to cancer genomics. Nucleic Acids Res. 2011; 39:e118. [PubMed: 21727090]
24. Liu X, Wang L, Zhao K, Thompson PR, Hwang Y, Marmorstein R, et al. The structural basis of protein acetylation by the p300/CBP transcriptional coactivator. Nature. 2008; 451:846–50. [PubMed: 18273021]
25. Maksimoska J, Segura-Peña D, Cole PA, Marmorstein R. Structure of the p300 histone acetyltransferase bound to acetyl-coenzyme A and its analogues. Biochemistry. 2014; 53:3415–22. [PubMed: 24819397]
26. Borbely G, Haldosen L-A, Dahlman-Wright K, Zhao C. Induction of USP17 by combining BET and HDAC inhibitors in breast cancer cells. Oncotarget. 2015; 6:33623–35. [PubMed: 26378038]
27. Martelotto LG, Ng CK, De Filippo MR, Zhang Y, Piscuoglio S, Lim RS, et al. Benchmarking mutation effect prediction algorithms using functionally validated cancer-related missense mutations. Genome Biol. 2014; 15:484. [PubMed: 25348012]
28. Janknecht R, Nordheim A. MAP kinase-dependent transcriptional coactivation by Elk-1 and its cofactor CBP. Biochem Biophys Res Commun. 1996; 228:831–7. [PubMed: 8941362]
29. Li Q-J, Yang S-H, Maeda Y, Sladek FM, Sharrocks AD, Martins-Green M. MAP kinase phosphorylation-dependent activation of Elk-1 leads to activation of the co-activator p300. EMBO J. 2003; 22:281–91. [PubMed: 12514134]
30. Kawahara T, Shareef HK, Aljarah AK, Ide H, Li Y, Kashiwagi E, et al. ELK1 is up-regulated by androgen in bladder cancer cells and promotes tumor progression. Oncotarget. 2015; 6:29860–76. [PubMed: 26342199]

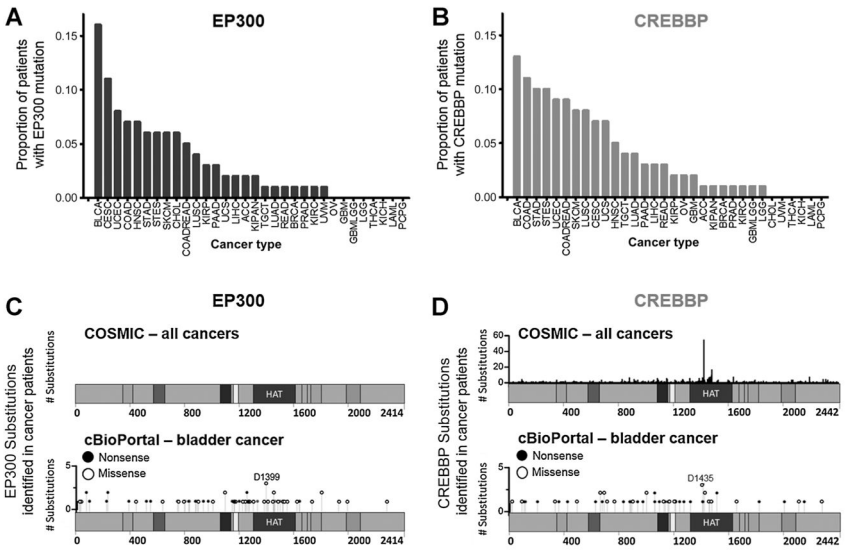

Figure 1.

EP300 and CREBBP patient identified mutations are most commonly found in bladder cancer patients and within the HAT domain of each gene. **A,** A total of 8,337 patients from 32 different cancer types were analyzed (The Cancer Genome Atlas) for mutations in EP300 and we found that bladder cancer patients had the highest frequency of mutations. **B,** As in **A**, we analyzed mutations in CREBBP and again found that bladder cancer patients had the highest frequency of mutations. **C,** Assessment of all known cancer-associated amino acid substitutions in EP300 as curated by COSMIC reveals that the HAT domain is the most mutated domain. Assessing bladder cancer patients specifically through TCGA using cBioPortal reveals the similar profile. **D,** The same mutational assessment in **C** was carried out on CREBBP and revealed identical conclusions.

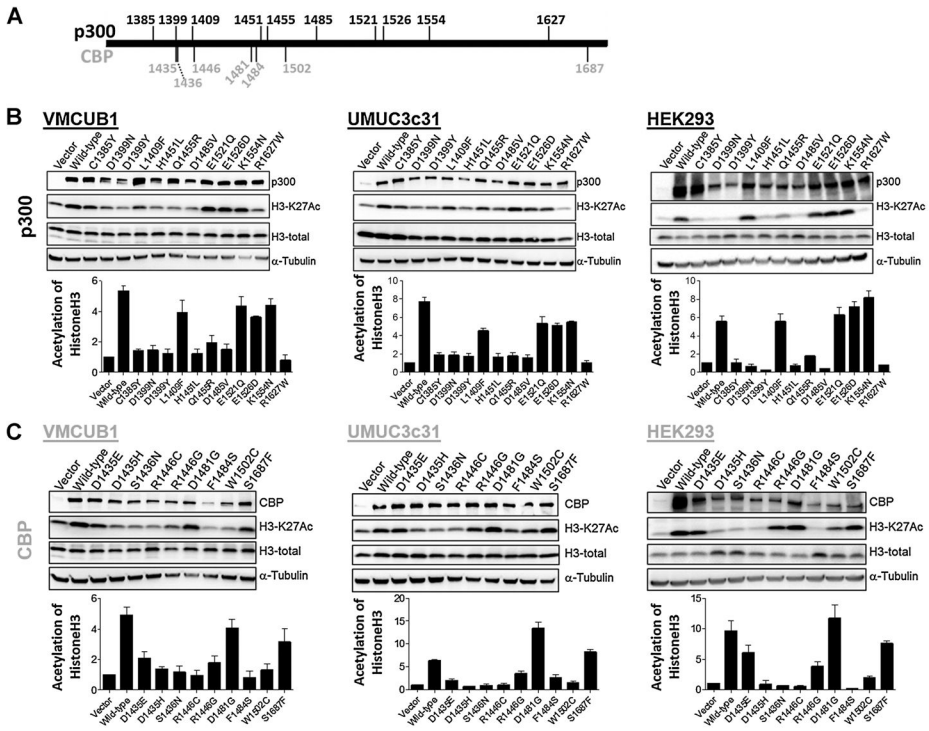

Figure 2.

Most missense mutations in the HAT domain of EP300 and CREBBP lead to HAT inactivation. **A,** Schematic showing the location of bladder cancer patient point mutations in p300 and CBP proteins relative to each other. Line is to scale. **B,** Each patient mutation was introduced into an EP300 construct which was then transfected into cells. Most, but not all, HAT domain point mutations lead to a loss of acetyltransferase activity as judged by the level of HistoneH3 acetylation at lysine 27. The blots are representative of three independent experiments in each cell line. Each graph shows the mean and standard error from the three independent experiments, with the data being normalized to vector alone (mean of 1). **C,** CREBBP HAT domain missense mutations analyzed as in **B**.

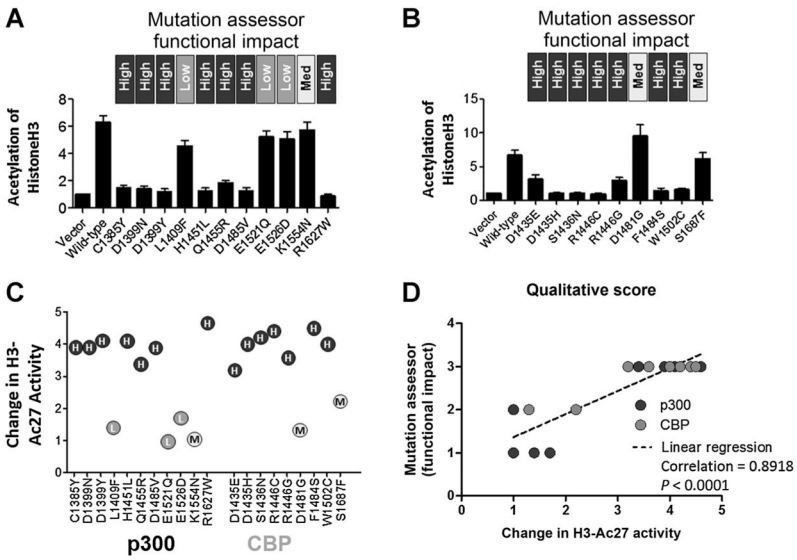

Figure 3.

The computer program Mutation Assessor predicted HAT activity of this bladder cancer patient dataset with 100% accuracy. **A,** The chart displays the mean and standard error of the 9 experiments performed above on p300 mutants in three cell lines. The Mutation Assessor functional impact label for each mutation is listed above the chart. **B,** Display of the mean and SE of 9 experiments performed above on CBP mutants in 3 cell lines. **C,** The difference in HistoneH3-Ac27 levels in a HAT domain mutant relative to the corresponding wild-type is plotted on the *y*-axis. For each mutation the value is represented as a circle, color coded as in **A** and **B** above to correspond to mutation assessor functional impact scoring. **D,** To mathematically assess correlation between observed acetyltransferase activity and Mutation Assessor prediction we assigned the Mutation Assessor designations numerical values: high = 3; medium = 2: low = 1. There is a strong correlation (Pearson) of 0.8918 between predicted HAT inactivity and decreased levels of acetylation of K27 of HistoneH3 ($P < 0.0001$).

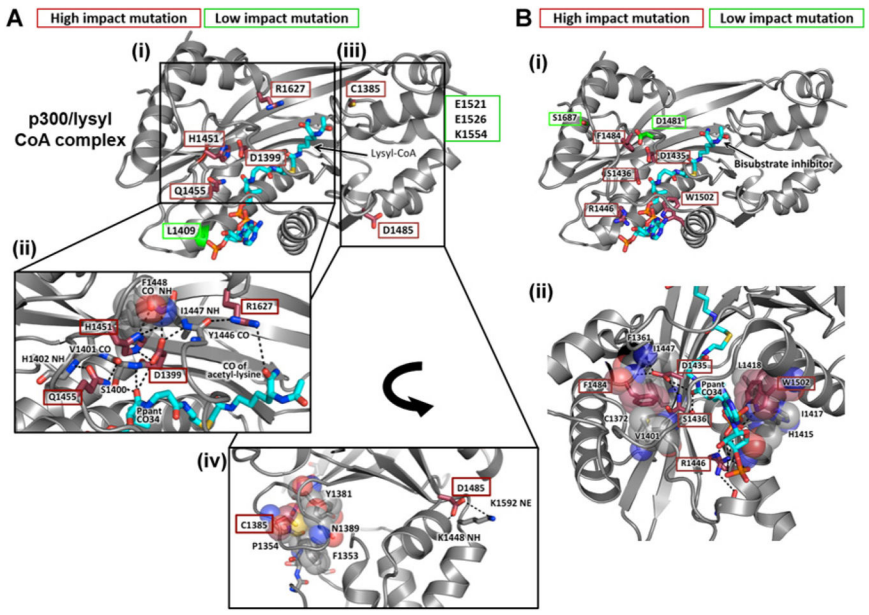

Figure 4.

Structural analysis of the missense mutants mapped onto the p300 HAT domain. **A,** Ribbon representation of the HAT domain colored in gray with the bisubstrate inhibitor shown in cyan. The high impact, in activating mutations are boxed in red while the low/medium impact, wild-type like mutations are boxed in green. Panel i and iii are a view of the p300 active site, detailing the environments of the deleterious mutation sites. Panel ii and iv are close-up views, with black dotted lines representing inferred hydrogen bonds. The surface rendering of amino acids highlights the role of the hydrophobic mutants in stabilizing hydrophobic pockets. **B,** Structural analysis of the missense mutants mapped onto the HAT domain from the CBP homology model. Panel i is a ribbon representation of the HAT domain, colored in gray, and the bisubstrate inhibitor colored in cyan. Panel ii is a close-up view of the p300 active site detailing the environments of the deleterious mutation sites.

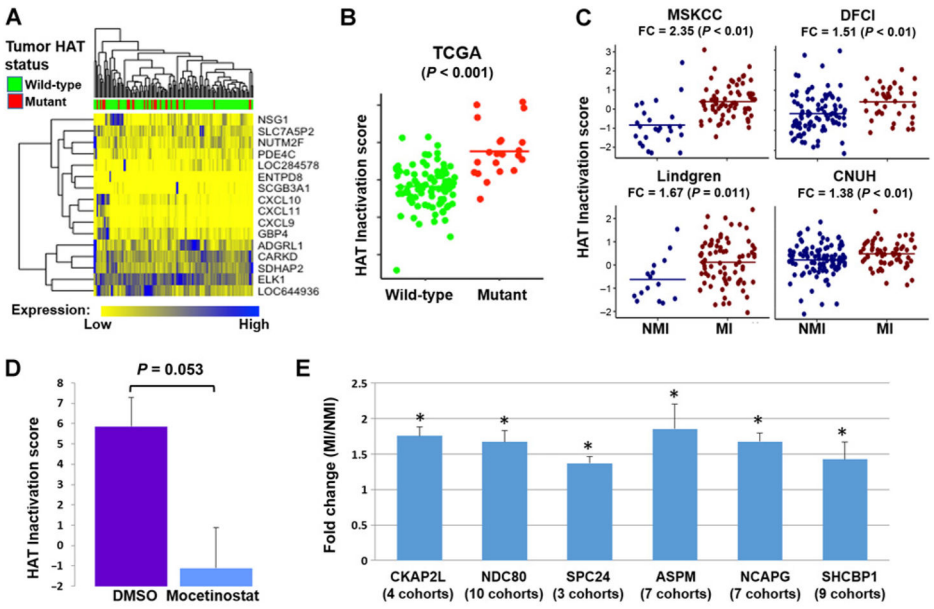

Figure 5.

Identification and clinical utility of a HAT inactivation signature in bladder cancer. **A,** Heatmap showing the 16 HAT inactivation signature genes and association with mutation status in the TCGA cohort. Signature genes are differentially expressed between HAT wild-type (green) and HAT mutant (red) ($P < 0.001$). For visualization, expression values for each gene are scaled to be between 0 (low expression; yellow) and 1(high expression; blue). **B,** Association between HAT inactivation score and HAT mutation status in the TCGA cohort. **C,** Association between HAT inactivation score and nonmuscle-invasive (NMI) and muscle-invasive (MI) tumors in bladder cancer in the CNUH ($n = 165$), DFCI ($n = 93$), Lindgren ($n = 130$), and MSKCC ($n = 91$) cohorts. **D,** Association between HAT inactivation score and treatment with histone deacetylase inhibitor mocetinostat. **E,** Genes downregulated following mocetinostat treatment (26) were evaluated for association with stage in bladder cancer, using the Bladder Cancer Biomarker Evaluation Tool (*BC-BET*). Bar graphs show the mean fold change (FC) for each gene, with FC > 1 indicating higher expression in muscle-invasive compared with nonmuscle-invasive tumors. *P* values are calculated using Fisher test to combine significance values from individual cohorts (also see Supplementary Table S1). Error bars, SEM.*, $P < 0.01$. *P* values in **B–D** are calculated using the two-sample *t* test.